Simulations of liquid crystals: bulk structure and interfacial properties

N. Akino[1], G. Germano[1], N. H. Phuong[1], F. Schmid[1], and M. P. Allen[2]

[1] Theoretische Physik, Universität Bielefeld,
D-33501 Bielefeld, Germany
E-mail: {germano, phuong, schmid}@physik.uni-bielefeld.de
hiroshi.akino@nifty.ne.jp
[2] Centre for Scientific Computing, University of Warwick,
Coventry CV4 7AL, United Kingdom
E-mail: M.P.Allen@warwick.ac.uk

We present large scale molecular dynamics simulations of liquid crystals, which are modeled as fluids of soft repulsive ellipsoidal molecules. In the first part of the paper, we discuss the bulk structure of nematic liquid crystals. The direct correlation function (DCF) has been determined for the first time in a nematic fluid without any approximations. We demonstrate that it can be used to calculate the Frank elastic constants, which are important phenomenological parameters in the continuum theory of liquid crystals. In the second part, we consider an interface between a nematic and an isotropic phase. The interplay between the surface tension and the elastic interactions in the nematic phase leads to an unusual fluctuation spectrum.

1 Introduction

Liquid crystals are beautiful examples of materials that are fascinating from a fundamental point of view – as complex fluids with intriguing symmetries and unusual elastic properties – and highly interesting for technological applications [1,2]. Like in most materials, many important properties depend on the structure of inhomogeneities and interfaces in the material. For example, the alignment of nematic liquid crystal on surfaces plays a key role in the domain of liquid crystal display devices [3,4,5]. For the theoretical physicist, interfaces in liquid crystals are appealing for yet another reason: Surfaces and interfaces break two continuous symmetries, the isotropy of space and the translational invariance. The interplay of this symmetry breaking with the broken symmetries in the various liquid crystal phases leads to a wealth of new intriguing phenomena [6,7,8,9,10]. Apart from discussing these effects from a phenomenological point of view, it is also interesting to investigate how they come about on a microscopic level, and to study the relation between the local structure of liquid crystals and relevant "mesoscopic" phenomenological parameters.

In this paper, we review some computer simulation work that we have done in this direction. We shall discuss the local structure and interfacial properties in two of the most important liquid crystal phases: The isotropic phase (I), which is an ordinary fully symmetric fluid phase, and the nematic phase (N), where the fluid has translational symmetry in all directions, but long range orientational order. Since we wish to restrict ourselves to these two phases, it is convenient to study a model which does not exhibit any other liquid

crystal phases – in particular, no smectic phases. We chose a simple idealized model of soft ellipsoids, which is particularly suited for large scale molecular dynamics simulations.

Our work pursues two goals: First, we seek to improve our understanding of local and large scale interfacial properties. Second, we wish to explore ways which allow to bridge between the microscopic structure – which is to some extent accessible to computer simulations of particle based models – and phenomenological theories, which operate on larger scales. Our paper will highlight some aspects of these two issues.

The paper is organized as follows: The model and the simulation method are presented in the next section. Then we discuss the local liquid structure in isotropic and nematic fluids and show how that knowledge can be used to evaluate elastic constants in a nematic liquid crystal. The procedure is based on a density functional result, which is originally due to Poniewiersky and Stecki [11]. It is an example of a procedure that bridges between local properties and phenomenological theories. In the third section, we describe results from large scale molecular dynamics simulations of a nematic-isotropic interface. Among other, we find an intriguing capillary wave spectrum, which reflects the complex interplay between the bare surface tension and the elastic interactions in the nematic phase. Finally, we summarize and discuss briefly the prospective future work.

2 Model, Method and Technical Details

Our model liquid crystal is defined as follows: We study soft ellipsoidal particles of mass m_0 with elongation $\kappa = \sigma_{\text{end-end}}/\sigma_{\text{side-side}}$. Two particles i and j with orientations $\mathbf{u}_i$ and $\mathbf{u}_j$ separated by the center-center vector $\mathbf{r}_{ij}$ interact via a purely repulsive pair potential,

$$V_{ij} = \begin{cases} 4\epsilon_0 \, (X_{ij}^{12} - X_{ij}^{6}) + \epsilon_0 & : X_{ij}^{6} > 1/2 \\ 0 & : \text{ otherwise} \end{cases} . \tag{1}$$

where $X_{ij} = \sigma_0/(r_{ij} - \sigma_{ij} + \sigma_0)$ and

$$\sigma_{ij} = \sigma_0 \left\{ 1 - \frac{\chi}{2} \left[\frac{(\mathbf{u}_i \cdot \hat{\mathbf{r}}_{ij} + \mathbf{u}_j \cdot \hat{\mathbf{r}}_{ij})^2}{1 + \chi \mathbf{u}_i \cdot \mathbf{u}_j} + \frac{(\mathbf{u}_i \cdot \hat{\mathbf{r}}_{ij} - \mathbf{u}_j \cdot \hat{\mathbf{r}}_{ij})^2}{1 - \chi \mathbf{u}_i \cdot \mathbf{u}_j} \right] \right\}^{-1/2} \tag{2}$$

with $\chi = (\kappa^2 - 1)/(\kappa^2 + 1)$. The function σ_{ij} approximates the contact distance between the two ellipsoids in the direction $\hat{\mathbf{r}}_{ij} = \mathbf{r}_{ij}/r_{ij}$ [12].

The systems were studied using a domain decomposition molecular dynamics program (GBMEGA). The simulations and parts of the data analysis (extensive evaluations of correlation functions) were carried out on the CRAYs T3E at NIC, using 128 and 256 processors in a typical run. The simulations were performed in the microcanonical ensemble using the RATTLE integrator [13], in rectangular simulation boxes with periodic boundary conditions in all directions. The time step Δt and the moment of inertia I depended on the elongation κ of the ellipsoids in the systems under consideration: For systems with $\kappa = 3$, we chose $\Delta t = 0.003\sqrt{m_0/\epsilon_0}\,\sigma_0$ and $I = 2.5\, m_0\, \sigma_0^2$, and for systems with $\kappa = 15$, $\Delta t = 0.002\sqrt{m_0/\epsilon_0}\,\sigma_0$ and $I = 50\, m_0\, \sigma_0^2$. Further simulation details will be given in the appropriate section.

We describe the orientation of an ellipsoid i by a unit vector $\mathbf{u}_i$. The nematic phase is then characterized by a nonzero order tensor [1]

$$\mathbf{Q} = \frac{1}{n}\sum_{i=1}^{n}\frac{1}{2}(3\mathbf{u}_i \otimes \mathbf{u}_i - \mathbf{I}), \tag{3}$$

where the sum i runs over all n particles of the system, $\mathbf{I}$ is the unit matrix and $\otimes$ the dyadic product of two vectors. The largest Eigenvalue of this matrix is the nematic order parameter S. The corresponding Eigenvector points in the direction of alignment. It is called the director $\mathbf{n}$.

In the following, we shall use scaled units defined in terms of σ_0, ϵ_0, m_0 and the Boltzmann constant k_B.

3 Bulk Structure and Elastic Constants

Before studying interfacial and surface properties of fluids, it is important to understand the local bulk structure of these fluids. A good knowledge of the local equilibrium structure allows one to calculate effective parameters, which in turn can be used in phenomonological theories to predict material properties on a larger scale.

On a phenomenological level, nematic liquid crystals are often described by the Frank free energy functional [14,15]

$$\mathcal{F}\{\mathbf{n}(\mathbf{r})\} = \frac{1}{2}\int d\mathbf{r}\Big\{K_{11}[\nabla\cdot\mathbf{n}]^2 + K_{22}[\mathbf{n}\cdot(\nabla\times\mathbf{n})]^2 + K_{33}[\mathbf{n}\times(\nabla\times\mathbf{n})]^2\Big\}. \tag{4}$$

Here it is assumed that the absolute value of the order parameter S is roughly constant throughout the system. Nevertheless, long wavelength fluctuations of the director $\mathbf{n}(\mathbf{r})$ must exist, because the nematic order breaks the isotropy of space, which is a continuous symmetry, and the Goldstone theorem applies [16]. The three contributions to the free energy functional – the splay mode (K_{11}), the twist mode (K_{22}), and the bend mode (K_{33}) – are illustrated in Figure 1. They are controlled by the Frank elastic constants K_{ii} and determine almost exclusively the structure and the properties of nematic liquid crystals on mesoscopic length scales.

On a microscopic level, the structure of fluids is described by N-particle distribution functions [17,18] and in particular by pair correlations. The central quantity in many theories of liquid matter is the so-called direct correlation function (DCF). It is defined as follows:

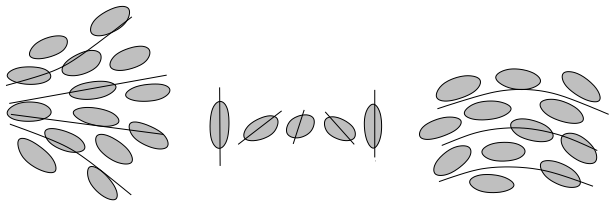

Figure 1:
Elastic modes in nematic liquid crystals

The starting point are the two-particle probability density $\rho^{(2)}(\mathbf{u}_1, \mathbf{r}_1, \mathbf{u}_2, \mathbf{r}_2)$ of finding simultaneously one particle of orientation $\mathbf{u}_1$ at the position $\mathbf{r}_1$, and another with orientation $\mathbf{u}_2$ at the position $\mathbf{r}_2$, and the one-particle probability density $\rho^{(1)}(\mathbf{u})$ of finding a particle with the orientation $\mathbf{u}$ at the position $\mathbf{r}$. In the bulk, $\rho^{(1)}$ is independent of $\mathbf{r}$, and $\rho^{(2)}$ depends only on the relative coordinates $\mathbf{r}_{12} = \mathbf{r}_1 - \mathbf{r}_2$. The correlations between two particles are described by the total correlation function

$$h(\mathbf{u}_1, \mathbf{u}_2, \mathbf{r}_{12}) = \frac{\rho^{(2)}(\mathbf{u}_1, \mathbf{u}_2, \mathbf{r}_{12})}{\rho^{(1)}(\mathbf{u}_1)\rho^{(1)}(\mathbf{u}_2)} - 1. \tag{5}$$

This function subsumes the direct effect of a particle 1 on a particle 2 and all the "indirect" effects mediated by the bulk of surrounding fluid. Due to the elasticity of the nematic fluid, it decays only slowly with an algebraic power law $1/r$. The long range correlations result from indirect contributions. In order to characterize the local structure, it thus seems desirable to separate "indirect" effects from "direct" effects. This is done by the Ornstein-Zernike equation [17,18]

$$h(\mathbf{u}_1, \mathbf{u}_2, \mathbf{r}_{12}) = c(\mathbf{u}_1, \mathbf{u}_2, \mathbf{r}_{12}) + \int c(\mathbf{u}_1, \mathbf{u}_3, \mathbf{r}_{13})\, \rho^{(1)}(\mathbf{u}_3)\, h(\mathbf{u}_3, \mathbf{u}_2, \mathbf{r}_{32}) d\mathbf{u}_3 d\mathbf{r}_3. \tag{6}$$

The DCF is the function $c(\mathbf{u}_1, \mathbf{u}_2, \mathbf{r}_{12})$. As it turns out, c is indeed short ranged even in the nematic phase.

The DCF is the starting point for several liquid state theories [17]. Many material constants can be calculated from the DCF. In nematic fluids, one is specially interested in the parameters which control the director profiles. Poniewierski and Stecki [11] have derived a set of expressions which relate the DCF with the elastic constants K_{ii}. These equations have been used a few times in the past to calculate elastic constants from simulations [19,20,21,22]. However, approximations were used for the form of the DCF, and the results therefore differed from values obtained by other methods for the same systems [23].

We have determined for the first time the exact direct correlation functions in a nematic fluid [24,25,26,27]. To this end, we have studied systems of up to 8000 soft ellipsoids at the number density $\rho = 0.3/\sigma_0^3$ and temperature $T = 0.5\ \epsilon_0/k_B$. This corresponds to a nematic state with the order parameter $\langle S \rangle = 0.69$. The phase transition to the isotropic phase occurs at $\rho = 0.29/\sigma_0^3$. For comparison, we have also calculated the DCF at the number density $\rho = 0.24/\sigma_0^3$, i.e., in an isotropic fluid. The run lengths were 5-10 million molecular dynamics steps.

All densities and correlation functions were expanded in spherical harmonics $Y_{lm}(\mathbf{u})$, in a frame where the z-axis points along the director.

$$\rho^{(1)}(\mathbf{u}) = \varrho \sum_{l \text{ even}} f_l\ Y_{l0}(\mathbf{u}) \tag{7}$$

$$F(\mathbf{u}_1, \mathbf{u}_2, \mathbf{r}_{12}) = \sum_{\substack{l_1, l_2, l \\ m_1, m_2, m}} F_{l_1 m_1 l_2 m_2 l m}(r)\, Y_{l_1 m_1}(\mathbf{u}_1)\, Y_{l_2 m_2}(\mathbf{u}_2)\, Y_{lm}(\hat{\mathbf{r}}_{12}). \tag{8}$$

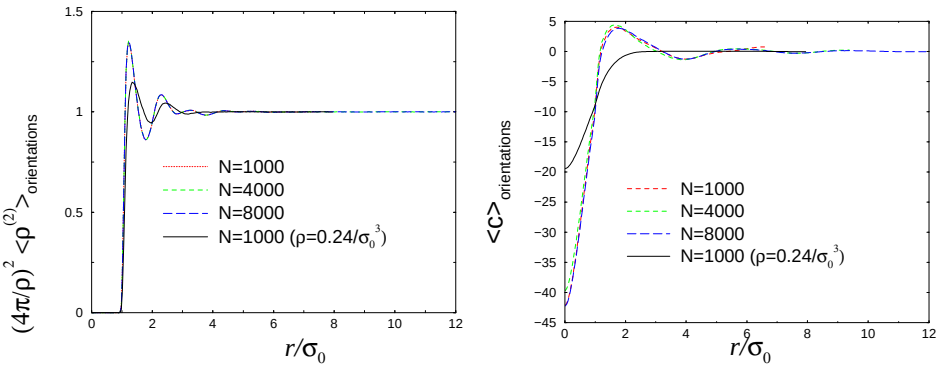

Figure 2:
Pair distribution function $\rho^{(2)}$ (left) and direct correlation function c (right) vs. molecular distance r, averaged over all orientations of $\mathbf{u}_i$,$\mathbf{u}_j$, and $\mathbf{r}_{ij}$, for different system sizes N, at the density $\rho = 0.3/\sigma_0^3$ (nematic phase). Solid black line shows corresponding curve for $\rho = 0.24/\sigma_0^3$ (isotropic phase) for comparison.

where $F = \rho^{(2)}$, h or c, $r = |\mathbf{r}_{12}|$, and $\hat{\mathbf{r}}_{12} = \mathbf{r}_{12}/r_{12}$. For symmetry reasons, all coefficients f_l and $F_{...}(r)$ are real, and only coefficients with $m_1 + m_2 = -m$ and even l_i enter the expansion.

The expansion coefficients of $\rho^{(2)}$ were computed from simulation configurations using [28]

$$\rho^{(2)}_{l_1 m_1 l_2 m_2 l m}(r) = 4\pi\, \varrho^2\, g(r)\, \langle\, Y^*_{l_1 m_1}(\mathbf{u}_1)\, Y^*_{l_2 m_2}(\mathbf{u}_2)\, Y^*_{l m}(\hat{\mathbf{r}})\, \rangle_{\delta r}, \tag{9}$$

where $g(r)$ is the radial distribution function, i.e. the number of molecular pairs at distances between r and $r + \delta r$, divided by $4\pi\varrho\, r^2 \delta r$. These time-consuming averages were calculated on a Cray T3E. We have determined coefficients for l_i, l up to $l_{max} = 6$ in all systems, and up to $l_{max} = 8$ in the smallest nematic system. A calculation with $l_{max} = 8$ requires the evaluation of 1447 different expansion coefficients of $\rho^{(2)}$ from the configuration data. Our computational resources did not permit to perform such a time consuming analysis in the larger systems. Choosing $l_{max} = 6$, we still had to calculate 469 different coefficients, which we did mostly on the CRAYs at NIC. The bin size was $\delta r = 0.04\sigma_0$.

Results for selected coefficients of $\rho^{(2)}$ and c are presented in Figures 2 and 3 [26]. Figure 2 shows orientational averages (over $\mathbf{u}_i$, $\mathbf{u}_j$, and $\mathbf{r}_{ij}$) of the pair distribution function and the DCF. Note that these curves are proportional to the coefficients $\rho^{(2)}_{000000}$ and $c_{000000}(r)$. The pair distribution does not look very different in the isotropic and the nematic phase. The DCF however reveals that the nematic phase has more hidden structure. Since we consider orientational averages, the long range algebraic correlations are not yet apparent: Both $\langle\rho^{(2)}\rangle$ and $\langle c\rangle$ are short ranged.

The effects of the elasticity become evident when looking at orientation dependent correlations. Figure 3 shows results for the expansion coefficients with $l_1 = l_2 = l = 2, m_1 = -m_2 = 1, m = 0$. In the case of $\rho^{(2)}$, this coefficient has a particularly pronounced long range tail. It disappears entirely in the corresponding curve for the DCF.

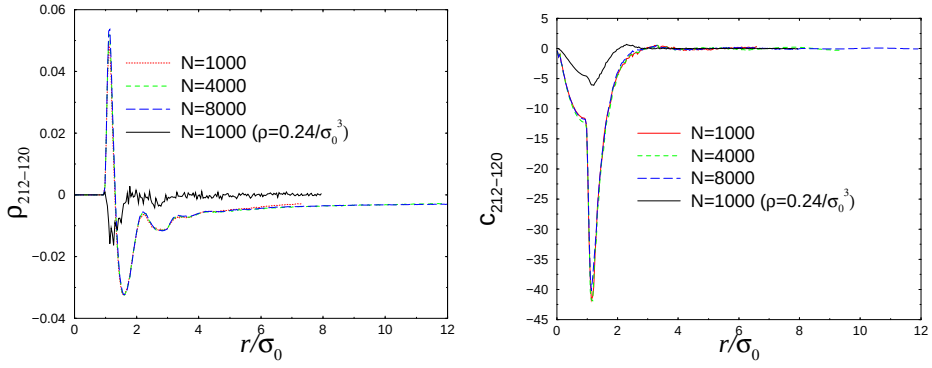

Figure 3:
Expansion coefficient with $l_1 = 2, l_2 = 2, m_1 = 1, m_2 = -1, l = 2$, and $m = 0$ of the pair distribution function $\rho^{(2)}$ (left), and the direct correlation function (right) vs. molecular distance r for different system sizes N at the density $\rho = 0.3/\sigma_0^3$ (nematic phase). Black solid line shows corresponding curve for $\rho = 0.24/\sigma_0^3$ (isotropic phase) for comparison.

Based on these results, we can establish the connection with the elastic constants in the nematic fluid. The Poniewierski-Stecki equations [11] are most conveniently evaluated in Fourier space. They can be written as [24]

$$K_{ii} = \frac{1}{2}\frac{d^2}{dk^2} C_{ii}(k)\Big|_{k=0} \qquad \text{for} \qquad i = 1, 2, 3, \tag{10}$$

where the $C_{ii}(k)$ are defined as

$$C_{ii}(k) = \frac{k_B T \varrho^2}{8\sqrt{\pi}} \sum_{l_1 l_2} \sqrt{l_1(l_1+1)}\sqrt{l_2(l_2+1)}\, f_{l_1}\, f_{l_2} \Big\{ [c_{l_1 1 l_2 -1 0 0}(k) + c_{l_1 -1 l_2 1 0 0}(k)]$$
$$+ v_i \frac{\sqrt{5}}{2}[c_{l_1 1 l_2 -1 2 0}(k) + c_{l_1 -1 l_2 1 2 0}(k)] + w_i \frac{\sqrt{15}}{\sqrt{8}}[c_{l_1 1 l_2 1 2 -2}(k) + c_{l_1 -1 l_2 -1 2 2}(k)] \Big\}$$

with $(v_1, v_2, v_3) = (-1, -1, 2)$, $(w_1, w_2, w_3) = (-1, 1, 0)$. The elastic constants K_{ii} can thus be determined from the initial slope of a plot of $C_{ii}(k)$ vs. k^2. Such a plot is shown in Figure 4. For comparison and as a check of our method, we have also performed an analysis of order tensor fluctuations following a method proposed by Allen et al [29,23]. To this end, we have performed additional molecular dynamics simulations of 4000 and 16000 particles in an ensemble where the director was constrained to be aligned along one side of the simulation box .

The results are summarized in Table 1. We have evaluated the pair distribution functions and calculated the DCF in systems of 1000, 4000, and 8000 particles. The upper cutoff l_{max} for the spherical harmonics expansion was chosen $l_{max} = 8$ in the smallest systems, and $l_{max} = 6$ in the others. Results for $l_{max} = 6$ and $l_{max} = 8$ were compared in the smallest system. They differed most critically in the value of K_{33}, but the difference is small (a few percent at $N = 1000$). As explained above, we were not able to carry out an analysis with $l_{max} = 8$ for all system sizes.

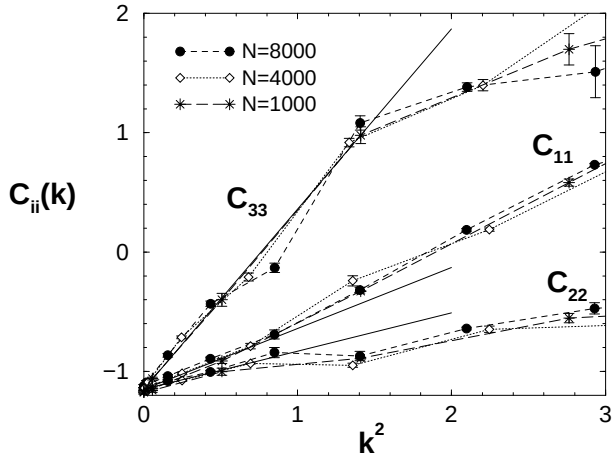

Figure 4:
Weighted sum of the DCF expansion coefficients $C_{ii}(k)$ as defined in Eqn. (10) vs. k^2 for different system sizes N. The initial slopes give the elastic constants K_{ii}. Thick solid lines indicate corresponding fits for the $N = 4000$ system.

Comparing the results for the elastic constants with those obtained from the analysis of order tensor fluctuations, we find that the values of K_{11} and K_{22} are identical for both methods. The DCF method slightly underestimates K_{33}, but since the value increases with l_{max}, this is probably an artefact of the cutoff in the spherical harmonics expansion.

Despite these systematic errors, the agreement between the values obtained from the two methods is reasonable. Hence we have established a practical way to apply the Poniewierski-Stecki equations to simulation data. It allows to calculate the elastic constants, which determine the mesoscopic structure of a nematic fluid, from the DCF, which characterizes its local liquid structure. Moreover, our findings give confidence in our results for the DCF. As a central quantity in density functional theory, the possible applications of the DCF go of course far beyond the calculations of elastic constants [17,30]. We plan to explore some of these in the future.

Table 1:
Elastic constants as obtained in systems with N particles with two methods. PS: Poniewerski-Stecki equations with DCF, calculated with a spherical harmonics expansion with an upper cutoff l_{max}; the results for $l_{max} < 6$ were about 20 % worse. OF: analysis of order tensor fluctuations. The statistical error on the last digit is given within parentheses.

N	method	l_{max}	$\langle K_{11} \rangle$	$\langle K_{22} \rangle$	$\langle K_{33} \rangle$
1000	PS	8	0.55 (2)	0.35 (3)	1.56 (4)
1000	PS	6	0.51 (2)	0.34 (3)	1.52 (4)
4000	PS	6	0.52 (2)	0.31 (1)	1.51 (3)
	OF		0.53 (1)	0.30 (1)	1.60 (1)
8000	PS	6	0.51 (2)	0.33 (2)	1.48 (3)
16000	OF		0.53 (1)	0.30 (1)	1.59 (1)

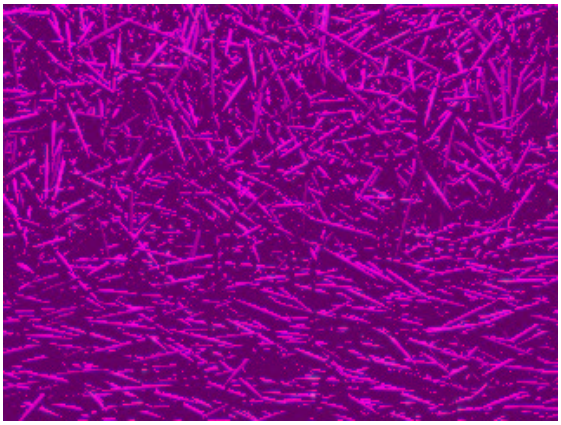

Figure 5:
Configuration snapshot of an interface between the nematic and the isotropic phase in a system of soft ellipsoids with elongation $\kappa = 15$.

4 The Nematic/Isotropic Interface

We turn to discuss interfacial properties in nematic liquid crystals. From a macroscopic point of view, the presence of surfaces or interfaces introduces three new effective parameters: the interfacial tension, the anchoring angle, and the anchoring energy. The anchoring angle is the director angle (with respect to the surface normal) favored by the surface. The anchoring energy is related to the force needed to twist the director out of the anchoring angle.

Our work at NIC currently concentrates on the study of interfaces between nematic and isotropic states (NI-interface). These interfaces are of fundamental interest, because they connect two fluid phases with a different symmetry. They are essential for wetting phenomena, which can be exploited to manipulate the anchoring at surfaces. They also play a key role for important nonequilibrium phenomena such as shear banding [31,32]. In all of these cases, the physics depends crucially on the structure and in particular on the fluctuations of the associated interfaces.

We have started with studying a free NI-interface. There have been a few simulations of NI-interfaces previously [34,35,36]. However, the systems were small, and fluctuation effects could not be studied. We considered a system with 115200 soft ellipsoids of elongation $\kappa = 15$. The high value of κ ensured a broad coexistence region: At the temperature $T = 1\epsilon/k_B$, the coexistence densities of the nematic and the isotropic phase were $\rho_N = 0.018/\sigma_0^3$ and $\rho_I = 0.016/\sigma_0^3$, respectively. The simulations were done in the microcanonical ensemble in a box geometry $(L_x : L_y : L_z) = (1 : 1 : 2)$ with periodic boundary conditions. The average density $\rho = 0.17/\sigma_0^3$ (i. e. $L_x = 150.2\sigma_0$) was chosen in the coexistence region. Thus the system phase separated into a nematic slab and an isotropic slab, with two interfaces in between. After a long equilibration procedure (see

Reference [33] for details), the systems were sampled over 3 million molecular dynamics steps.

A snapshot of part of a configuration is shown in Figure 4. One recognizes the nematic side (bottom), the isotropic side (top), and the interface between the two. The anchoring on the nematic side is planar, i. e., the particles are aligned parallel to the interface on average. One also recognizes strong fluctuations of the position of the interface (capillary waves). These clearly have to be taken into account when studying the interfacial structure.

The simplest theory of interfacial fluctuations, the capillary wave theory [37], presumes that the local position of the interface can be parametrized by a unique function $h(x, y)$, and that the fluctuations of h are controlled solely by the interfacial tension γ. Under that assumption, the (two-dimensional) Fourier modes of h are distributed like

$$\langle |h(\mathbf{q})|^2 \rangle = k_B T/(\gamma q^2). \tag{11}$$

The capillary waves broaden the interfacial region. The apparent interfacial width ω is predicted to depend on the lateral size $L_\parallel$ like

$$\omega^2 = \omega_0^2 + \frac{k_B T}{4\gamma} \ln(L_\parallel/b_0), \tag{12}$$

where b_0 is a microscopic reference length, and ω_0 is the interfacial width on that length scale.

In order to study these effects, we have divided the simulation box in columns of size $B \times B \times L_z$ and calculated the two local interface positions h in each block. Profile averages were then computed with respect to the distance to the closest interface. Figure 6 (left) shows the resulting order parameter profiles for different block sizes B. The apparent width of the interface increases with the block size B. We have determined the interfacial width ω by fitting the profiles to a tanh-function. In a plot of ω^2 as a function of the block size B (Figure 6, right), we recover the logarithmic growth predicted by the capillary wave

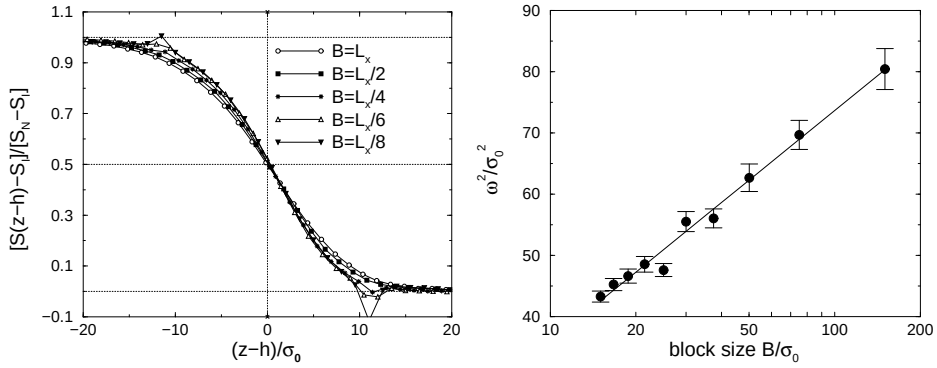

Figure 6:
Left: Order parameter profiles for different block sizes as indicated. S_N and S_I denotes average values of the order parameter in the nematic and the isotropic phase, respectively.
Right: Squared interfacial width ω^2 vs. block size B.

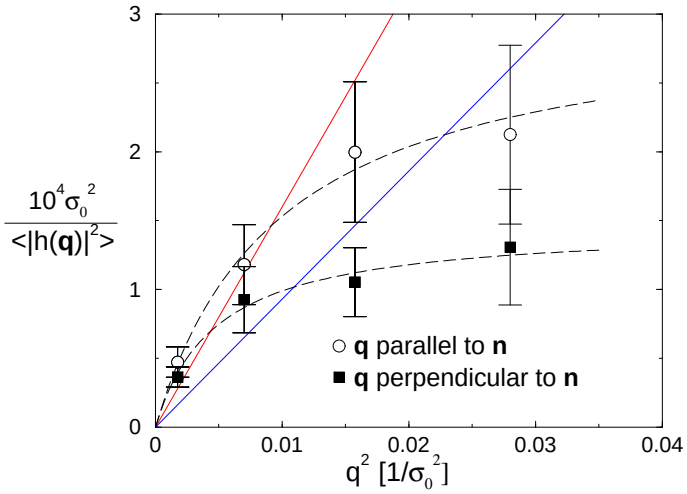

Figure 7:
Inverse of mean-squared Fourier components of the interface position, $1/\langle|h(\mathbf{q})|^2\rangle$, vs. square of the wave vector q^2, for wavevectors pointing parallel (circles) and perpendicular (squares) to the director. Dashed lines are guides to the eye. Solid lines are predictions of the capillary wave theory (11) with $\gamma = 0.016\ \sigma_0^2/k_BT$ (upper, blue line) and $\gamma = 0.0093\ \sigma_0^2/k_BT$ (lower, red line).

theory (12 with $L_\parallel = B$). From the slope of the straight line, one can estimate the interfacial tension, $\gamma = 0.016 \pm 0.002\ k_BT/\sigma_0^2$.

The capillary wave spectrum $h(\mathbf{q})$ was analyzed from the landscape of interfacial positions h at a fixed block size $B = L_z/8$. Figure 7 plots the results for $1/\langle|h(\mathbf{q})|^2\rangle$ versus q^2. Comparing these data with the equation (11), one notices that the prediction of the simple capillary wave theory does not describe the interface quite as well as the results for the interfacial broadening made us believe. First, the fluctuations of the interfacial position are anisotropic: They are much larger in the direction perpendicular to the director than in the parallel direction. Second, the amplitude of the fluctuations is larger than expected on small length scales (large q), and smaller than expected on large length scales ($q \to 0$). The discrepancy with the capillary wave prediction on large length scales becomes even worse if we use an independent estimate of the interfacial tension, $\gamma = 0.0093\ \sigma_0^2/k_BT$, which was calculated from the anisotropy of the pressure tensor [36].

Hence the simulations reveal an unexpectedly complex capillary wave spectrum. In fluids with purely short-range interactions, the capillary wave theory (11) usually describes fluid-fluid interfaces quite well on large length scales. The discrepancies observed here suggest that the effectively long-range elastic interactions in the nematic phase influence the interfacial fluctuations significantly. One can speculate that they might even suppress them entirely in the limit of infinitely long particles [33] (Onsager limit [38,39]). These relations between elastic properties and fluctuations shall be explored in more detail in the future. Obviously, they are not only important for the nematic-isotropic interface, but more generally for all surfaces of nematic fluids.

5 Conclusions and Outlook

To summarize, we study the structure and properties of liquid crystals by molecular dynamics simulations. As for all materials, a global understanding of the properties of liquid crystals requires simulations on many different length scales and levels of coarse graining. Our simulations operate on a coarse grained microscopic level: The length scale is microscopic, yet details of the molecular structure are disregarded. The purpose of our studies is twofold: On the one hand, we aim at a better understanding of the relationship between the microscopic, local structure, and the mesoscopic properties of inhomogeneous liquid crystals: For example, we have demonstrated that the DCF can be used to bridge between the microscopic length scale and higher levels of coarse graining, in which only effective parameters like the elastic constants matter. On the other hand, we explore physical phenomena which are characteristic for our length scale – such as the specific properties of interfacial fluctuations on the length scale of a few molecular lengths.

Our future work shall follow these lines. We plan to study the relationship between the local structure at surfaces and the phenomenological parameters which describe surface anchoring. Here again, density functional approaches which make use of DCF information seem promising. Furthermore, we believe that the unusual fluctuation spectrum which we have observed in equilibrium interfaces will lead to a wealth of new phenomena in nonequilibrium interfaces, i. e., interfaces under shear.

Acknowledgements

We have benefitted from discussions and interactions with K. Binder, A. McDonald, and H. Lange. The work presented here was carried out using extensive computer time on the CRAYs T3E of the NIC (Jülich). Altogether, we have used roughly 200.000 processor hours (400.000 billing units). The parallel program GBMEGA was originally developed by the EPSRC Complex Fluids Consortium, UK. Our work was supported by the German Science Foundation (DFG).

References

1. P.-G. de Gennes and J. Prost, *The Physics of Liquid Crystals* (Oxford University Press, Oxford, 1995).
2. S. Chandrasekhar, *Liquid Crystals* (Cambridge University Press, Cambridge, 1992).
3. B. Jerome, Rep. Progr. Phys. **54**, 391 (1991).
4. B. Bahadur (edt.) *Liquid crystals and uses*, World Scientific, Singapore (1990).
5. M. Schadt, Ann. Rev. Mater. Science, **27**, 305 (1997).
6. J. Cognard, *Alignment of Liquid Crystals and their Mixtures* (Gordon and Breach, London, 1982).
7. N. L. Abbott, in Curr. Opn. in Coll. Interf. Sci. **2**, 76 (1997).
8. J. Papanek, Ph. Martinot-Lagarde, *J. Phys. II France* **6**, 205 (1996).

9. D.E. Sullivan, R. Lipowski, *Can. J. Chem.* **66**, 553 (1988).
10. F.N. Braun, T.J. Sluckin, E. Velasco, *J. Phys.: Condens. Matter* **8**, 2741 (1996).
11. A. Poniewierski and J. Stecki, Mol. Phys. **38**, 1931 (1979); Phys. Rev. A **25**, 2368 (1982).
12. J. B. Berne, P. Pechukas, J. Chem. Phys. **56**, 4213 (1971).
13. H. C. Andersen, J. Comput. Phys. **52**, 24 (1983).
14. C. Oseen, Trans. Faraday Soc. **29**, 883(1933); H. Zöcher, ibid. **29**, 945 (1933).
15. F. C. Frank, Discuss. Faraday Soc. **25**, 19 (1958).
16. J. Goldstone, Nuovo Cimento **19**, 154 (1961); J. Goldstone, A. Salam, S. Weinberg Phys. Rev. **127**, 965 (1962).
17. J. P. Hansen and I. R. McDonald, *Theory of Simple Liquids* (Academic Press, London, 1986).
18. C. G. Gray and K. E. Gubbins, *Theory of Molecular Fluids*, Vol. 1 (Oxford, New York, 1984).
19. J. Stelzer, L. Longa, and H. R. Trebin, J. Chem. Phys. **103**, 3098 (1995); ibid., **107**, 1295 (1997).
20. J. Stelzer, L. Longa, and H. R. Trebin, Mol. Cryst. and Liq. Cryst. **262**, 455 (1995).
21. J. Stelzer, M. A. Bates, L. Longa, and G. R. Luckhurst, J. Chem. Phys. **107**, 7483 (1997).
22. A. V. Zakharov and A. Maliniak, Eur. Phys. J. E **4**, 85 (2001).
23. M. P. Allen, M. A. Warren, M. R. Wilson, A. Sauron, and W. Smith, J. Chem. Phys. **105**, 2850 (1996).
24. N. H. Phuong, G. Germano, F. Schmid, J. Chem. Phys. **115**, 7227 (2001).
25. N. H. Phuong, G. Germano, F. Schmid, submitted to Comp. Phys. Comm. (2001).
26. N. H. Phuong, Dissertation Universität Bielefeld, in preparation (2002).
27. N. H. Phuong, F. Schmid, manuscript in preparation (2002).
28. W. B. Streett and D. J. Tildesley, Proc. Roy. Soc. Lond. A 348, 485-510 (1975).
29. M. P. Allen and D. Frenkel, Phys. Rev. A **37**, 1813 (1988); ibid. **42**, 3641E (1990).
30. R. Evans, in *Fundamentals of Inhomogeneous Fluids*, p. 86, D. Henderson ed. (Marcel Dekker, New York, 1992).
31. P.D. Olmsted, P.M. Goldbart, *Phys. Rev. A* **46**, 4966 (1992); P.D. Olmsted, C.-Y. D. Lu, Faraday Discuss. **112**, 183 (1999); P.D. Olmsted, Europhys. Lett. **48**, 339 (1999).
32. G. Porte, J.-F. Berret, J.L. Harden, *J. Phys. II France* **7**, 459 (1997).
33. N. Akino, F. Schmid, M. P. Allen, Phys. Rev. E **63**, 041706 (2001).
34. M. A. Bates and C. Zannoni, Chem. Phys. Lett. **280**, 40 (1997).
35. M. P. Allen, J. Chem. Phys. **112**, 5447 (2000).
36. A. J. McDonald, M. P. Allen, F. Schmid, Phys. Rev. E **63**, 10701R (2001).
37. J. D. Weeks, J. Chem. Phys. **67**, 3106 (1977); D. Bedeaux and J. D. Weeks, J. Chem. Phys. **82**, 972 (1985).
38. L. Onsager, Ann. N.Y. Acad. Sci. **51**, 627 (1949).
39. Y. Mao, M. E. Cates, H. N. W. Lekkerkerker, J. Chem. Phys. **106**, 3721 (1997).